SPECT/CT Imaging of [111]Ag for the Preclinical Evaluation of Silver-Based Antimicrobial Nanomedicines

Colin Blackadar, Ka-Yee Grace Choi, Mary F. Embree, Heather M. Hennkens,
Cristina Rodríguez-Rodríguez, Robert E. W. Hancock, Katayoun Saatchi,* and Urs O. Häfeli*

Cite This: https://doi.org/10.1021/acsami.2c03609
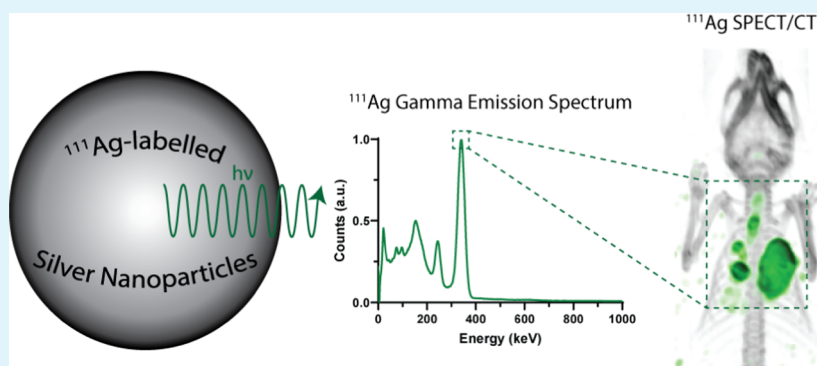
Read Online

ACCESS | 📊 Metrics & More | 📖 Article Recommendations | 🆂🅸 Supporting Information

[111]Ag SPECT/CT

[111]Ag Gamma Emission Spectrum

ABSTRACT: With the growing interest in developing silver-based antimicrobials, there is a need to better understand the behavior of silver within biological systems. To address this, we showed that single-photon emission computed tomography (SPECT) is a suitable method to noninvasively image [111]Ag-labeled compounds in mice. Formed by neutron irradiation of palladium foil, [111]Ag can be rapidly isolated with a high degree of purity and stably incorporated into antimicrobial silver nanoparticles. The imaging showed that nanoparticles are retained in the lungs for up to 48 h following intratracheal instillation, with limited uptake into the systemic circulation or organs of the reticuloendothelial system. Furthermore, in a mouse model of pulmonary *Pseudomonas aeruginosa* infection, the nanoparticles reduced the bacterial burden by 11.6-fold without inducing the production of pro-inflammatory mediators. Overall, SPECT imaging with [111]Ag is a useful tool for noninvasively visualizing the biodistribution of silver-containing compounds in rodents. This knowledge of how silver nanoparticles distribute *in vivo* can be used to predict their therapeutic efficacy.

KEYWORDS: antimicrobial, nanoparticles, silver, silver-111, imaging, SPECT/CT

■ INTRODUCTION

The antimicrobial activity of silver is well-established.[1,2] With increased resistance to conventional antibiotics, there has been an interest in developing silver-based antimicrobials, which show excellent results even against multidrug-resistant bacteria.[3] Colloidal silver nanoparticles (AgNPs) are the most widely studied silver-based antimicrobial, although silver-containing organometallic complexes,[4,5] polymeric nanoparticles,[6,7] and metal-organic frameworks[8,9] have all been reported with antimicrobial activities. Despite claims that silver is minimally toxic to humans,[10,11] silver can induce oxidative stress and DNA damage in mammalian cells.[12−14] Additionally, bioaccumulation of silver has been detected in marine animals.[15] Because of these concerns, there is a need to develop techniques to study silver-containing materials in mammalian systems.

We are interested in noninvasively imaging silver compounds *in vivo* to discover their tissue distribution and pharmacokinetics. This has been performed in microscopic marine organisms using fluorogenic Ag^+ sensors and optical microscopy.[16,17] These techniques, however, have limited translatability to larger animal systems. In mouse models, silver imaging thus far has mainly relied on indirect radio- or fluorescent labeling to generate a detectable probe.[18−20] These types of studies rely on the assumption that the silver compound and label remain conjugated *in vivo*. Multiple studies, however, have shown that the primary mechanism of action of silver-based antimicrobials is through Ag^+ release, so it is inherent within the design of these materials that the active
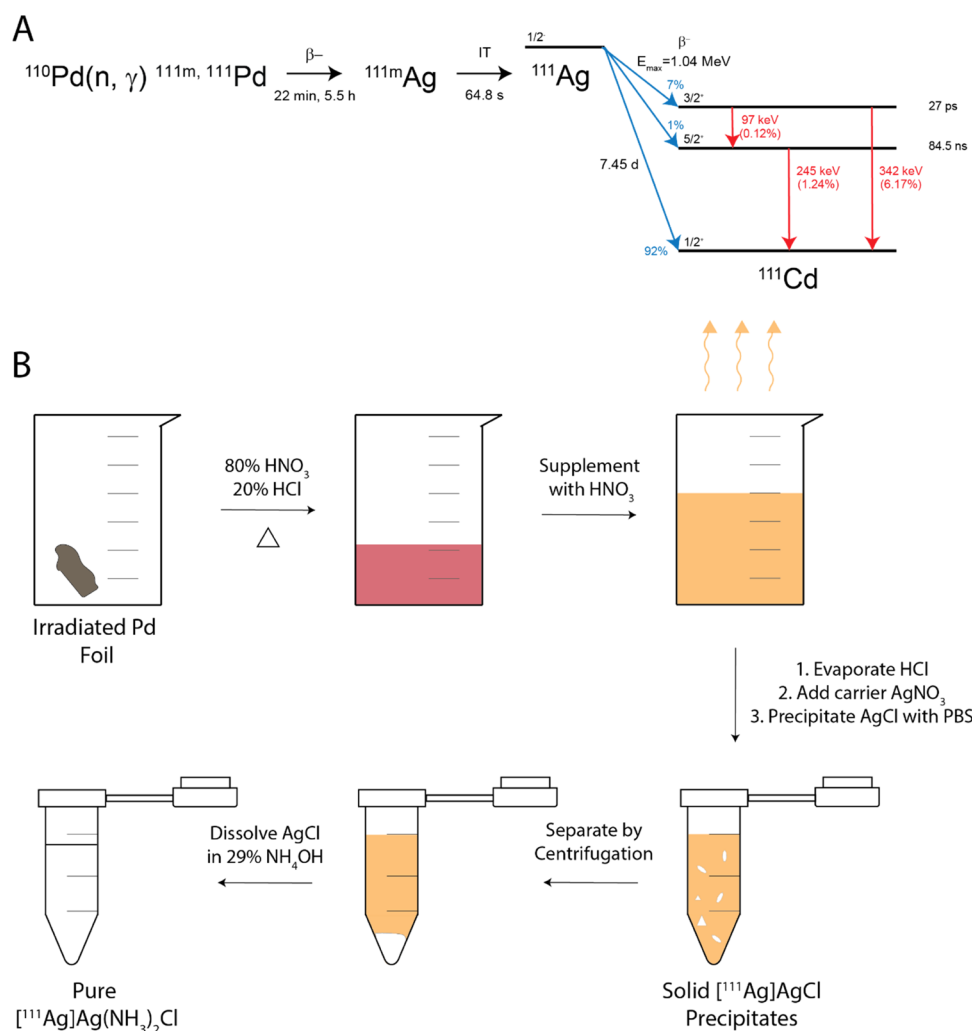
Figure 1. Preparation of ^{111}Ag for silver nanoparticle radiolabeling. (A) Neutron activation and decay scheme of ^{111}Ag. Data are from NuDat 3.0 (https://www.nndc.bnl.gov/nudat3/). (B) Scheme for the separation of ^{111}Ag from neutron-irradiated palladium foil.

agent is released from the probe.[21,22] It is, therefore, critical to specifically measure the silver component of these compounds.

Nuclear imaging with a radioisotope of silver would allow for the unambiguous detection of silver with a noninvasive imaging modality. The isotope ^{111}Ag suits this purpose. It has a half-life of 7.45 days and undergoes 100% β decay (E_{max} = 1.04 MeV) into stable ^{111}Cd, with two main γ emissions at 245 keV (1.0%) and 342 keV (7.1%).[23] These γ emissions are suitable for detection by single-photon emission computed tomography (SPECT).[23,24] ^{111}Ag can be produced by neutron irradiation of ^{110}Pd to generate ^{111m}Pd and ^{111}Pd,[25,26] both of which give rise to ^{111}Ag by β decay and an isomeric transition through a short-lived ^{111m}Ag intermediate.[25,26] The production and decay scheme for ^{111}Ag is shown in Figure 1A. To date, there are only a handful of studies that have used ^{111}Ag for studying silver in biological systems, and we could not find any that performed ^{111}Ag SPECT imaging. Aweda et al. used ^{111}Ag γ counting to quantify the biodistribution of silver-loaded polymeric nanoparticles and silver carbene complexes in mice.[27,28] Chattopadhyay et al. used ^{111}Ag-labeled hydroxyapatite particles for radio synovectomy treatment of joint inflammation.[29] They observed retention of their particles in the joint using γ camera imaging.[29]

The aim of this study was to evaluate SPECT/CT as a method to noninvasively image silver-based antimicrobials in vivo. Here, we developed and optimized a simple and rapid procedure to isolate ^{111}Ag from neutron-irradiated palladium and incorporate it into colloidal AgNPs. We administered the radiolabeled nanoparticles intratracheally to mice and imaged them at multiple time points up to 48 h with SPECT/CT to determine their tissue distribution. Lastly, we evaluated the antimicrobial activity of the AgNPs in vitro and in vivo in a mouse model of pulmonary Pseudomonas aeruginosa infection. Overall, this paper highlights the utility of ^{111}Ag SPECT imaging in the preclinical evaluation of silver-based antimicrobials and shows how it can guide the design of silver-based therapeutics.

■ RESULTS AND DISCUSSION

Separation of ^{111}Ag from Neutron-Irradiated Palladium Foil. ^{111}Ag was formed by neutron irradiation of an isotopically enriched ^{110}Pd foil (Figure 1A).[30] Prior to AgNP synthesis, the desired silver isotope had to be isolated from the palladium. Complete removal of palladium was particularly important since the AgNP synthesis produced particles with a different size distribution in the presence of trace amounts of palladium (Supporting Information, Figure S1A).
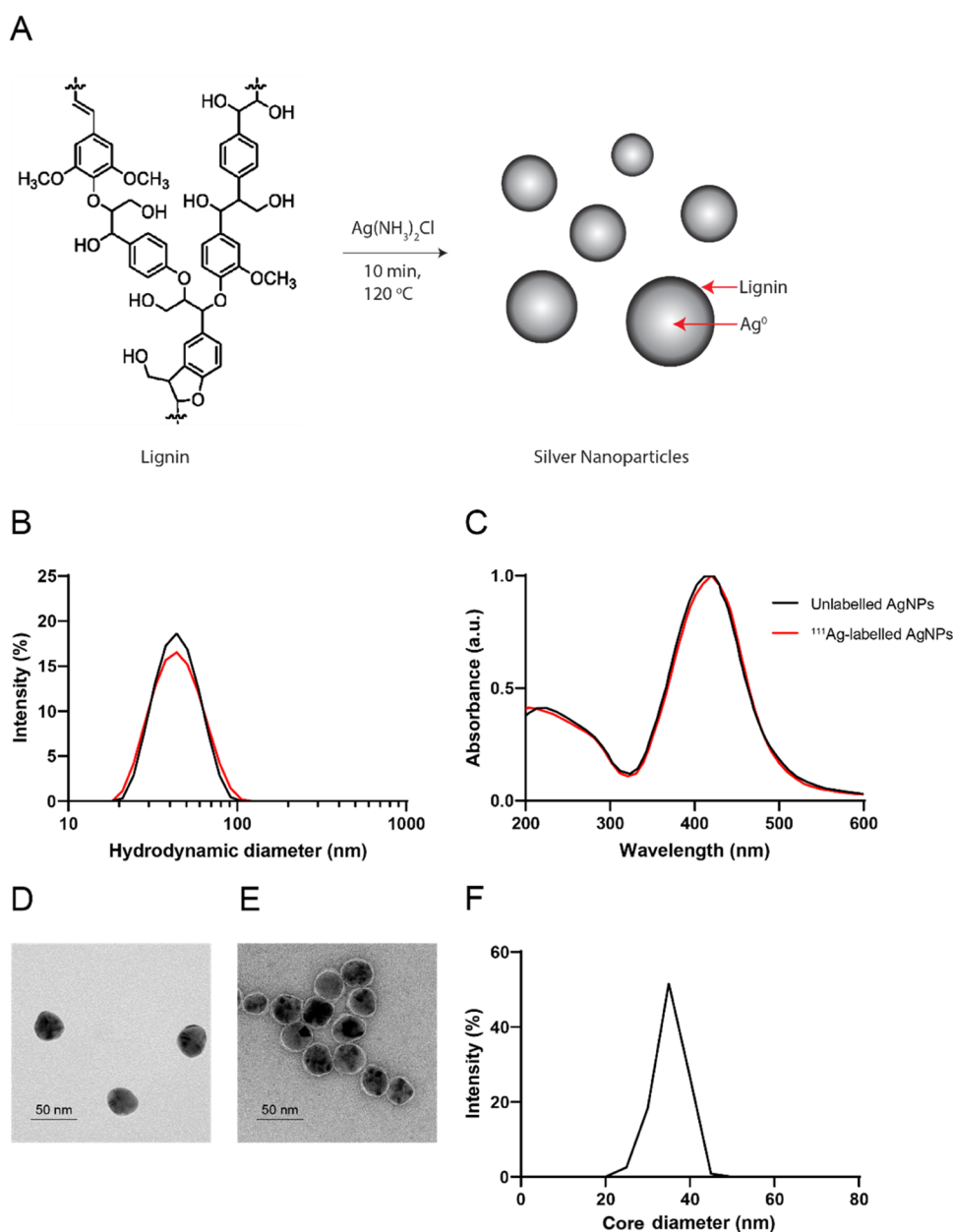
Figure 2. Synthesis and characterization of unlabeled and [111]Ag-labeled AgNPs. (A) Scheme for the synthesis of AgNPs from silver diamine chloride using lignin as a reducing and capping agent. (B) Intensity percent size distribution of unlabeled and [111]Ag-labeled AgNPs in water measured using dynamic laser light scattering (DLS). (C) UV−vis spectra of unlabeled and [111]Ag-labeled AgNPs. (D) TEM image of unlabeled AgNPs. (E) TEM image of unlabeled AgNPs with a uranyl acetate negative stain to visualize the lignin coating. (F) Core AgNP diameter measured from the TEM images, n = 120 nanoparticles.

A carrier-added protocol was used for this separation, which is outlined in Figure 1B. The palladium foil and [111]Ag were first dissolved and oxidized to Pd^{2+} and Ag^+ in a mixture of nitric and hydrochloric acids. Once the hydrochloric acid had evaporated, nonradioactive silver nitrate was added as a carrier to allow for the precipitation of the [111]Ag as silver chloride. Because palladium chloride salts are highly soluble, the solid silver chloride could then be isolated. It was then redissolved in ammonium hydroxide to generate silver diamine chloride $[Ag(NH_3)_2Cl]$. This procedure was performed in under an hour with a [111]Ag recovery of 93% and a palladium removal of >99.99% (Supporting Information, Figure S1B). It is noteworthy that cadmium, the decay product of [111]Ag, is also

soluble as a chloride salt, so any decayed [111]Ag contaminants would also be removed with this protocol.[31]

Synthesis and Characterization of [111]Ag-Labeled AgNPs. In our previously reported synthesis of AgNPs, lignin, a naturally occurring phenolic polymer from plants, was used as a reducing and capping agent, with silver nitrate as the silver source.[32] These AgNPs could be synthesized in 10 min using microwave irradiation to rapidly heat the mixture to 120 °C.[32] The [111]Ag separation procedure produced soluble silver diamine chloride. While there are many ways to convert this silver form to silver nitrate,[33−35] we found that AgNPs could be formed from silver diamine chloride directly under otherwise identical reaction conditions to our previous synthesis. The scheme for this synthesis is shown in Figure
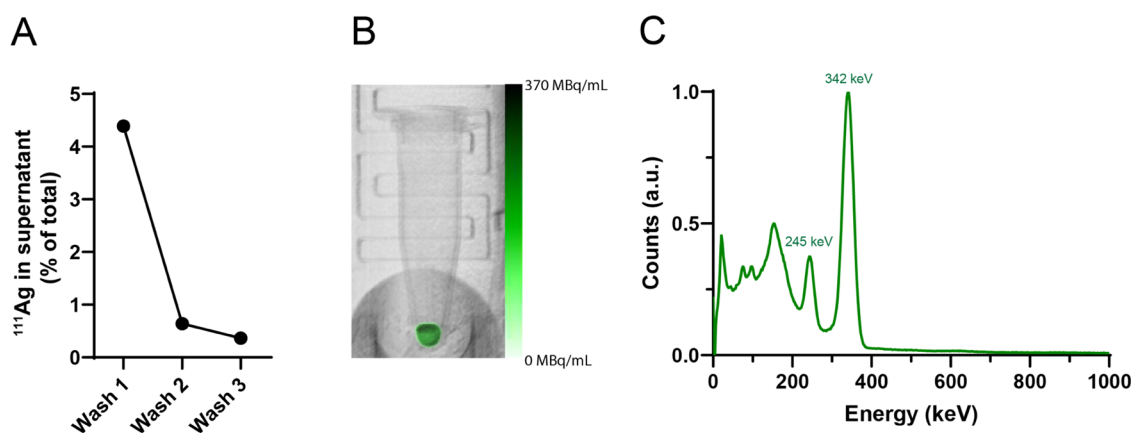
Figure 3. Characterization of [111]Ag-labeled AgNPs for SPECT imaging. (A) Quantification of [111]Ag in wash supernatants during the purification of crude particles. Minimal [111]Ag was detected after the first wash, showing that [111]Ag was stably incorporated into the particles. (B) SPECT/CT image of [111]Ag-labeled AgNPs in a test tube. (C) γ spectrum of photons detected during the acquisition of the image in (B).

Table 1. Antimicrobial Activities of AgNPs Diluted in 50% Water and 50% Mueller−Hinton Broth against Different Bacterial Strains[a]

media: 50% water/50% MHB	MIC (μg/mL)			MBC (μg/mL)		
	batch 1	batch 2	batch 3	batch 1	batch 2	batch 3
P. aeruginosa LESB58	2−4	2	2	4−8	8	8
P. aeruginosa LESB65	1−2	1	2	2−8	4	8
P. aeruginosa PA01	4−8	4−8	8	4−16	8	8
S. aureus USA300	>128	>128	>128	>128	>128	>128
A. baumannii	4−8	4−8	8	8−16	4	8
K. pneumoniae	64−128	>128	>128	>128	>128	>128

[a]MIC, minimal inhibitory concentration; MBC, minimal bactericidal concentration.

2A. The AgNPs had a hydrodynamic diameter of 36 ± 6 nm and polydispersity index of 0.125 ± 0.03 (mean ± SD of 6 batches) (Figure 2B). The ζ-potential of the particles was −52 ± 8 mV (mean ± SD of 4 batches). The AgNPs displayed the characteristic surface plasmon resonance (SPR) absorption for AgNPs at 420 nm (Figure 2C).[36] When viewed with transmission electron microscopy (TEM) (Figure 2D), the particles had an average core diameter of 33 nm (Figure 2F). The lignin coating was visible with a negative stain and was approximately 2 nm thick (Figure 2E). X-ray diffraction analysis of the AgNPs confirmed that silver was only in the reduced Ag^0 oxidation state (Supporting Information, Figure S2). The particles were stable in water and showed no signs of silver leeching or aggregation after two months of storage (Supporting Information, Figure S3). The AgNPs formed aggregates in saline and phosphate-buffered saline (PBS) (Supporting Information, Figure S4). In serum, the particles acquired a protein corona which stabilized them from forming the larger structures observed in saline and PBS (Supporting Information, Figure S4). The hydrodynamic diameter of serum-coated AgNPs was roughly stable when incubated at 37 °C up to 48 h, after which it began to decrease (Supporting Information, Figure S5). When uncoated particles were incubated in water at 37 °C, the particle size was stable up to 13 days (Supporting Information, Figure S5).

When [111]Ag was incorporated into the AgNPs to make [[111]Ag]AgNPs, there was no change in the particle characteristics (Figure 2B,C). The radiochemical yield for the synthesis was 83.9%. When this synthesis was performed with non-radioactive silver, the yield was 84.0 ± 11.4% (mean ± SD of 3 batches), which is very much in line with the radiochemical

yield. During purification of the crude product by ultra-centrifugation, there were negligible amounts of [111]Ag in the supernatants past the first wash (Figure 3A). This indicates that the radioisotope was stably incorporated into the AgNPs.

***In Vitro* Evaluation of AgNP Antimicrobial Activity.** The lignin-capped AgNP synthesis was slightly modified from previous studies due to the way we extracted [111]Ag. To confirm the antimicrobial activity of the AgNPs produced from silver diamine chloride, we compared them to lignin-capped AgNPs produced from silver nitrate, which were highly active against a variety of organisms.[32] Activity against *P. aeruginosa* and *Acinetobacter baumannii* was high in AgNPs produced with silver diamine chloride, with minimal inhibitory concentrations (MICs) and minimal bactericidal concentrations (MBCs) in the low μg/mL range (Table 1). Activity against *K. pneumoniae* and *Staphylococcus aureus* was lower, as found in other studies on AgNPs.[37,38] There was minimal variability in the antimicrobial activity between batches, and the activity in the low μg/mL range was retained after one month of storage (Supporting Information, Table S1).

SPECT/CT Imaging of [[111]Ag]AgNPs. To determine the suitability of [[111]Ag]AgNPs for SPECT, a quantity of known activity and radionuclidic purity as determined using a High Purity Germanium (HPGe) detector (Mirion Technologies (Canberra) Inc., Atlanta, GA) with Genie 2000 software was imaged in a test tube (Figure 3B), and a γ spectrum was acquired (Figure 3C). The γ spectrum contained the expected photopeaks at 245 and 342 keV. As we used the high-energy collimator, the more abundant 342 keV peak was used to calculate a calibration factor for quantitative *in vivo* imaging.
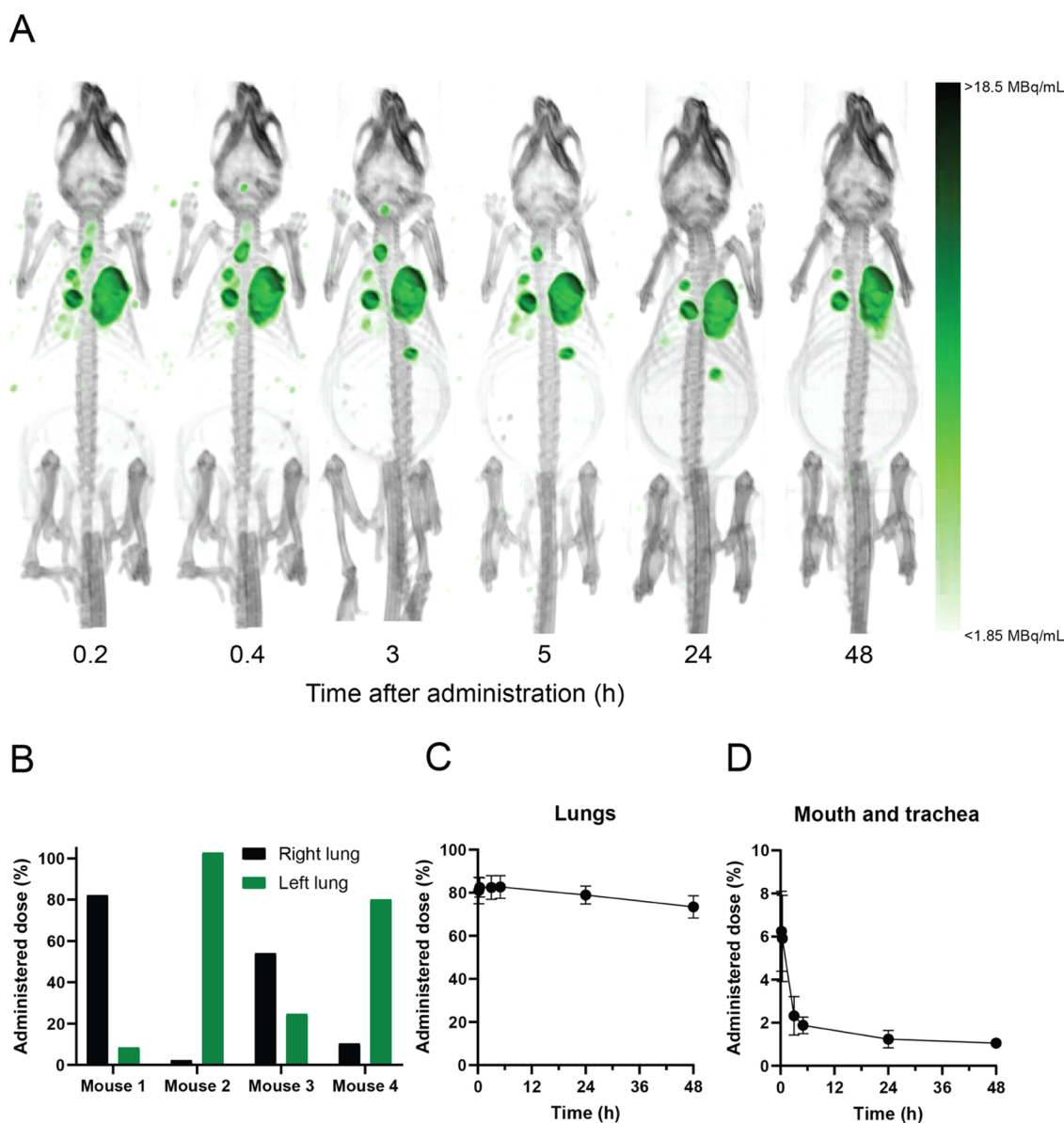
Figure 4. SPECT image analysis of intratracheally administered [111Ag]-labeled AgNPs in mice. C57BL/6 mice were administered 4.0 mg/kg (13.1 MBq) [111Ag]AgNPs via intratracheal instillation and were imaged with SPECT/CT up to 48 h. (A) Representative SPECT/CT renderings of the [111Ag] signal at each time point. (B) Quantification of the asymmetric [111Ag] distribution between lungs for each mouse at the 0.2 h time point. (C) Quantification of [111Ag] signal in the lungs as a percentage of the administered dose; $n = 4$, mean $\pm$ SD. (D) Quantification of the residual [111Ag] dose in the mouth and trachea; $n = 4$, mean $\pm$ SD.

[111Ag]AgNPs were administered intratracheally to healthy female C57BL/6 mice, and the mice were imaged using SPECT up to 48 h post administration. A full-body computed tomography (CT) scan was performed following each scan to allow for anatomical localization of the [111Ag] signal. Each mouse received, on average, 13.1 MBq of [111Ag], which equates to a silver dose of 4.0 mg/kg. This dose was well tolerated by all mice and did not induce any visible signs of respiratory distress. Figure 4A shows representative SPECT/CT images acquired at each time point. The [111Ag]AgNPs were primarily deposited in the lungs, averaging 81.0 $\pm$ 6.2% of the administered dose (% AD) immediately after administration. The distribution of particles in the lungs was asymmetric (Figure 4B), which is typical for the intratracheal instillation method used.[39] Most particles were retained in the lungs for the duration of the study, with 73.5 $\pm$ 5.2% AD remaining after

48 h (Figure 4C). High lung retention following pulmonary deposition has been reported for many AgNPs, though there is considerable variability between residence times.[40,41] Particle size and surface coating play a large role in the elimination kinetics. For perspective, Anderson et al. found that 98% of citrate-coated AgNPs were retained in the lung after 21 days, while only 9% of poly(vinylpyrrolidone)-coated AgNPs were retained in the same time frame.[40] Since many AgNPs with different coatings and sizes have been reported, comparisons between studies are difficult.

The rest of the dose was deposited in the mouth and trachea during the placement and removal of the catheter−syringe system for the intratracheal instillation. Some mouth and trachea deposition was also due to internal back splashing of the suspension and partial exhaling, which cannot be completely avoided. An average of 6.2 $\pm$ 1.9% AD was
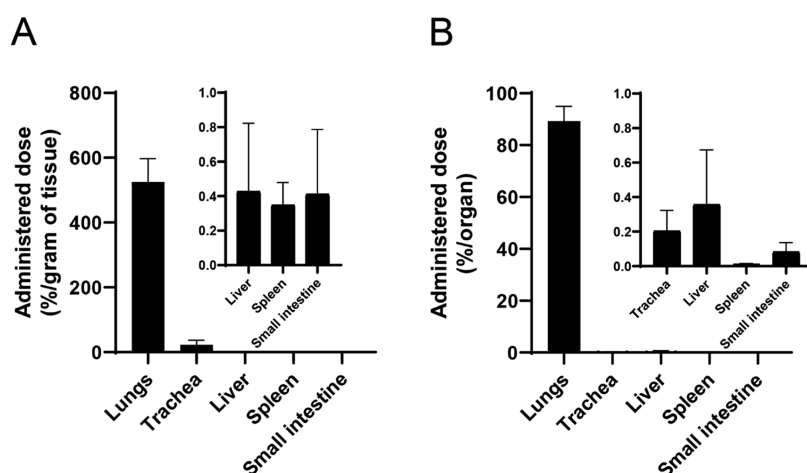
A

B

Figure 5. Biodistribution of intratracheal ^{111}Ag-labeled AgNPs in mice 48 h after administration. C57BL/6 mice were administered 4.0 mg/kg (13.1 MBq) [^{111}Ag]AgNPs via intratracheal instillation. After 48 h, the mice were sacrificed, and organs were removed for ^{111}Ag quantification with γ counting. (A) ^{111}Ag concentration in organs expressed as % AD/g of tissue; $n = 4$, mean $\pm$ SD. (B) ^{111}Ag concentration in organs expressed as % AD/organ $n = 4$, mean $\pm$ SD.

deposited in the mouth and trachea (Figure 4D). Most of this was removed within 24 h, with 1.2 $\pm$ 0.40% AD still present at this time point. This remained more or less constant for the remainder of the study, with 1.1 $\pm$ 0.19% AD present at the final 48 h time point. The radiation signal in the gastrointestinal tract (mainly the stomach) after 3 h suggests that some of the AgNPs deposited in the mouth and throat were swallowed (Figure 4A). An additional contribution came likely from the large airways, where AgNPs moved by mucociliary clearance upward and were then swallowed. This has been reported for other inhaled nanomaterials.[42]

Biodistribution of [^{111}Ag]AgNPs. After 48 h, the mice were sacrificed, organs were harvested, and the amount of ^{111}Ag in each organ was quantified with γ counting. Organs with the highest ^{111}Ag content are shown in Figure 5 while the rest of the organs are shown in the Supporting Information, Table S2. Consistent with the image analysis, most of the [^{111}Ag]AgNPs were in the lungs (89.3 $\pm$ 5.7% AD), though the image analysis reported a value 18% lower than this. After the lungs, the organ with the highest silver concentration was the trachea (22.9 $\pm$ 14.1% AD/g), with very minor amounts in the liver (0.43 $\pm$ 0.40% AD/g), small intestine (0.41 $\pm$ 0.37% AD/ g), and spleen (0.35 $\pm$ 0.13% AD/g).

Uptake into the organs of the reticuloendothelial system (RES), namely the liver and spleen, was expected. The RES is well-known for its efficiency in clearing the blood of nanomaterials, and previous studies have shown high uptake into the RES for intravenously-administered AgNPs.[19] Any lung-deposited AgNPs that were absorbed into systemic circulation would have likely been cleared by RES macrophages. The low [^{111}Ag]AgNP concentration in the RES (<1% AD/g) as well as minimal AgNP content in the blood (0.18 $\pm$ 0.12% AD/g at 48 h) suggests that few AgNPs were systemically absorbed.

***In Vivo* Evaluation of AgNP Antimicrobial Activity.** The AgNPs showed strong antimicrobial activity against three *P. aeruginosa* strains and were particularly effective against the epidemic cystic fibrosis clinical isolate LESB65 *in vitro* (Table 1). With the imaging results showing excellent lung retention, we hypothesized that the AgNPs would be effective at treating pulmonary infections. To test this, we evaluated the

antimicrobial activity of AgNPs in an established mouse model of acute *P. aeruginosa* infection.[43] AgNPs administered intranasally at a single dose of 5 mg/kg reduced the bacterial burden by 11.6-fold after 24 h (Figure 6). Smaller doses of 0.5
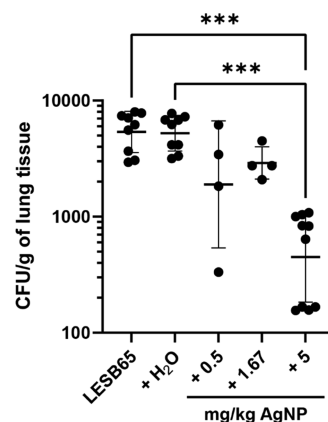

Figure 6. AgNPs significantly reduced bacterial load in a murine model of *P. aeruginosa* infection. *P. aeruginosa* LESB65-Lux ($\sim$10^7 CFU) were inoculated dropwise into the left naris of CD-1 mice. Mice were treated with endotoxin-free H$_2$O (vehicle control) or 0.5, 1.67, or 5 mg/kg AgNPs 24 h post nfection. Lung homogenates were used to enumerate bacterial burden; $n \geq 4$ mice per group, geometric mean $\pm$ geometric SD, *** $p < 0.001$, according to Kruskal–Wallis test, followed by Dunn's correction.

and 1.67 mg/kg also reduced the bacterial burden, though the results were not statistically significant (Figure 6). When the particles were administered to uninfected mice at 5 mg/kg, there was no induction of the pro-inflammatory mediators MCP-1, KC, IL-6, and IL-1α (Figure 7). In addition, the particles did not alter the levels of *P. aeruginosa*-induced pro-inflammatory cytokines (Figure 7). This suggests that the AgNPs exerted a direct antimicrobial effect instead of killing bacteria through the modulation of host inflammation. Treatment of infected mice with AgNPs did not reduce the amount of pro-inflammatory mediators in the lung.

The *in vivo* bactericidal activity of AgNPs has been studied in mouse models of gastrointestinal, intraperitoneal,[44] and
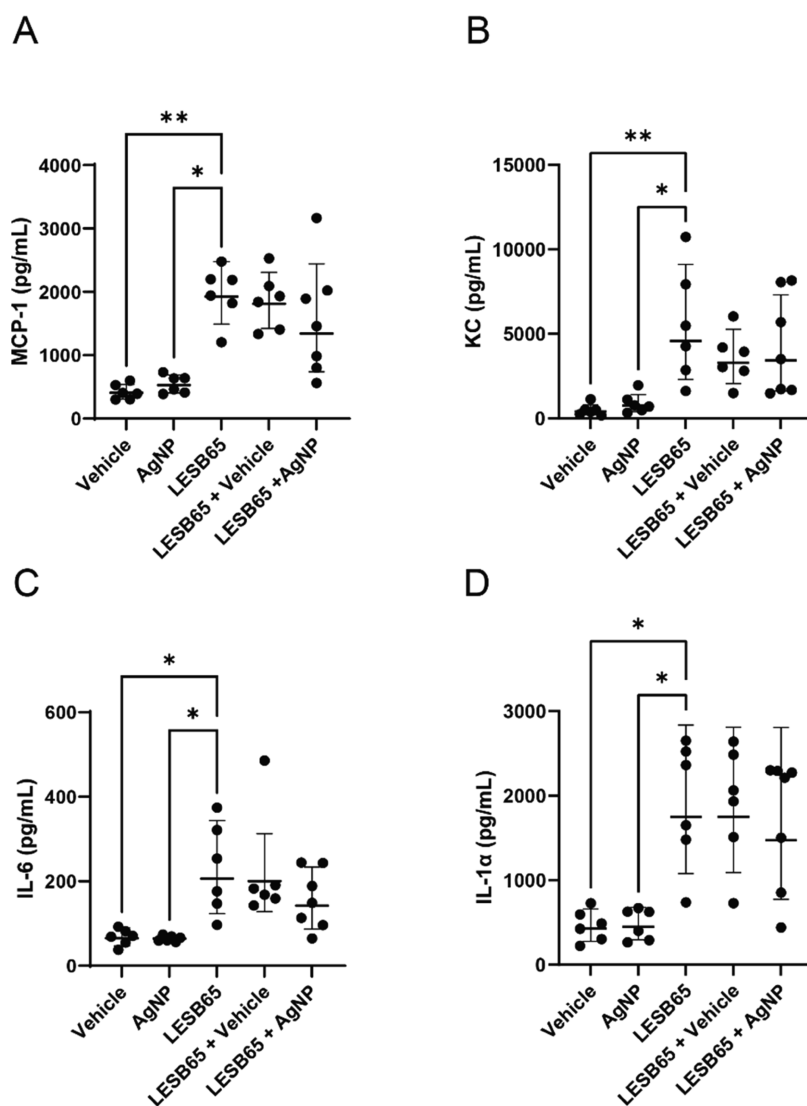
F

Figure 7. AgNPs did not modulate bacterial-mediated immune responses. *P. aeruginosa* LESB65-Lux ($\sim 10^7$ CFU) was inoculated dropwise into the left naris of CD-1 mice. Mice were treated with endotoxin-free H_2O (vehicle) or 5 mg/kg AgNPs 24 h post infection. Lung homogenates were used to determine the production of chemokines (A) MCP-1, (B) KC/CXCL1 and pro-inflammatory cytokines, (C) IL-6, and (D) IL-1α; $n \geq 6$ mice per group, geometric mean ± geometric SD, * $p < 0.05$, ** $p < 0.01$, according to Kruskal−Wallis test, followed by Dunn's correction.

cutaneous infection.[45,46] While we found one report of a polymeric system designed to release silver in a mouse lung bacterial infection model, we could not find any literature that used colloidal AgNPs in a lung bacterial infection model.[47] A wide range of *in vivo* antimicrobial activities has been reported for AgNPs, with reductions in bacterial burden ranging from 3-fold to greater than 100-fold.[44−48] Differences in nanoparticle characteristics, dose, infection model, and route of administration contribute to this wide range of results in the literature. Our AgNPs caused an 11.6-fold reduction in *P. aeruginosa* in the lungs. While this value is well within the range of reported *in vivo* AgNP activities, it is lower than that found in some studies. Our group has recently used SPECT to compare three different modes of pulmonary administration, and intranasal administration resulted in an average lung deposition of 29%.[49] With this knowledge, roughly 36 μg of the administered AgNPs should have reached the lungs, resulting in a concentration of 180 μg/g based on an average lung mass of 0.2 g. Since this value is much larger than the MBC of these AgNPs against this *P. aeruginosa* strain, the *in*

vivo bacterial clearance could have been higher. This argument, however, assumes a homogeneous distribution in the lungs, which likely did not occur *in vivo*.[49,50] It is possible that the AgNPs formed areas of focal accumulations in the lungs with high levels of bacterial killing, while bacteria continued to grow in spaces devoid of the AgNPs. The use of a spraying device could be employed in future studies to assure a more homogeneous lung distribution.[50] In addition, AgNPs and other nanomaterials are rapidly taken up by alveolar macrophages.[40,41,51] The resultant reduced levels of extracellular AgNPs in the lung could have reduced their effective concentration below the MBC of the AgNPs. Delivery of AgNPs to the infected sites in the lung, therefore, remains a barrier to the development of AgNP-based antimicrobials. Lastly, our study only evaluated the antimicrobial activity of the AgNPs after a 24-h treatment. With our imaging data showing that the AgNPs are still present in high amounts up to 48 h, it is possible that more pronounced antimicrobial effects could have been observed by increasing the treatment time.

Future studies should evaluate the antimicrobial activity of these AgNPs at later time points.

Many studies have shown that AgNPs are pro-inflammatory in the lungs, though this was not observed in our case. This was unexpected since our dose of 5 mg/kg was high compared to doses that other groups have used to show inflammatory responses in the lungs to AgNPs.[52−56] The pulmonary response to AgNPs is characterized by a large influx of neutrophils, an increase in protein content in bronchoalveolar lavage fluid, and the release of pro-inflammatory mediators.[52−55] Although we did not specifically measure neutrophil levels, the chemokine KC is secreted by mast cells and macrophages in the lungs and plays an important role in neutrophil recruitment.[53,57,58] It was not upregulated when our AgNPs were administered. There is less of a consensus on the MCP-1 and IL-6 response to AgNPs, with some studies showing they are upregulated and some showing they are unchanged.[53,54,59] Our data suggests that the current dose of AgNPs does not mediate an acute inflammatory response 1 day post administration. It is possible that AgNPs may induce a delayed immune response similar to a previous study by Botelho et al., which observed upregulation of pro-inflammatory mediator expression after 3 days post-AgNP administration but not after 1 day.[56] Future studies should evaluate the effects of these AgNPs in the lungs on a longer timescale.

CONCLUSIONS

We were interested in validating SPECT imaging as an effective method to image [111]Ag-labeled silver antimicrobials. To do this, we optimized a protocol for the separation of [111]Ag from neutron-irradiated palladium and subsequently incorporated the radioisotope into lignin-capped AgNPs. These AgNPs were intratracheally instilled into mice, which underwent a series of SPECT/CT acquisitions for the following 2 days. The images showed high retention of the AgNPs in the lung, and we detected minimal (<1% AD/g) uptake into the systemic circulation, the liver, or the spleen in the time frame of this study. We then evaluated the antimicrobial activity of the AgNPs in a mouse *P. aeruginosa* infection model with the rationale that high lung retention would allow for efficient bacterial killing. Within 24 h, the AgNPs caused an 11.6-fold reduction in the bacterial burden in mice, and the nanoparticles showed no pro-inflammatory activity. This study identifies an important role of [111]Ag SPECT imaging in the preclinical development of silver antimicrobials.

METHODS

Separation of [111]Ag from the Irradiated Palladium Target. [111]Ag was produced from [110]Pd at the University of Missouri Research Reactor (MURR) by direct neutron capture via the irradiation of metallic [110]Pd foil targets. Briefly, a piece of enriched [110]Pd foil (98.99% enrichment) weighing 1.18 mg was irradiated for 99.22 h in a sealed quartz vial in the MURR flux trap ($\sim$1.8 × 10^{14} n cm^{-2} s^{-1} thermal neutron flux position). Eight days after the end of irradiation, the target (124.7 MBq) was dissolved in 500 μL of 1:4 concentrated hydrochloric acid: concentrated nitric acid within 1−2 min with light heating ($\sim$50 °C), then 2 mL of concentrated nitric acid was added, and the solution was gently evaporated to $\sim$800 μL to expel any hydrochloric acid. This solution was diluted with 300 μL of water, then 50 μL of 118 mM silver nitrate was added. Silver was isolated by the addition of 200 μL of phosphate-buffered saline (PBS) at pH 7.4 to precipitate silver chloride. The solid AgCl was separated by centrifugation, then dissolved in 200 μL of 29% ammonium hydroxide. To generate ultrapure silver chloride, the solution was diluted with 1 mL of water, then silver chloride was re-precipitated by the addition of 200 μL of conc. hydrochloric acid. This AgCl was separated by centrifugation and dissolved in 29% ammonium hydroxide. The separation efficiency was determined by performing this procedure in triplicate with nonradioactive palladium and quantifying the palladium content in the purified solutions using a fluorescent palladium detection kit (EIAPDAPIF, Thermo Fisher Scientific). Quantification of [111]Ag was performed using a CRC-55tR dose calibrator (Capintec).

Synthesis of Lignin-Capped AgNPs. Silver chloride was produced by addition of PBS to aqueous silver nitrate and isolated by centrifugation. The solid silver chloride was dissolved in 29% ammonium hydroxide to a concentration of 29.5 mM, and a 1% (w/v) solution of lignin was made in water. The silver chloride and lignin solutions were mixed with a silver chloride: lignin volume ratio of 2:3. This mixture was then heated to 120 °C in an Initiator Microwave Synthesizer (Biotage) for 10 min. The crude particles were collected by ultracentrifugation (15,000 rcf × 10 min) and were washed with ultrapure water until the pH was between 7 and 8 (typically 2−3 washes). Nanoparticle concentrations were determined by lyophilizing (Labconco Freezone 2.5 Plus, Kansas City, MO) a known volume in a preweighed test tube overnight and then weighing the amount of powder left over. For the [111]Ag-labeled AgNPs, 101.1 MBq of [[111]Ag]AgCl (17.3 MBq/μmol on day of synthesis) in 200 μL 29% ammonium hydroxide was reacted with 300 μL of 1% lignin.

Characterization of Lignin-Capped AgNPs. *UV−Vis Spectroscopy.* UV−vis spectra of AgNP solutions were measured using a Nanodrop 2000 spectrophotometer (Thermo Scientific). AgNPs were measured at a concentration of roughly 10 μg/mL in water. Absorbance values were normalized by the absorbance at 420 nm, the wavelength of the characteristic surface plasmon resonance (SPR) band for silver, centered between 400 and 422 nm.[36,60]

Dynamic Light Scattering and ζ-Potential. Hydrodynamic diameter and ζ-potential measurements were made in water using a Malvern Zetasizer ZS 3600 (Malvern PANalytical, Malvern, U.K.).

Transmission Electron Microscopy. Transmission electron microscopy was performed at the University of British Columbia Bioimaging Facility. Images were acquired on an FEI Tecnai G20 TEM (FEI Company, Hillsboro, OR). AgNPs in water were deposited on a Formvar/Carbon coated 200 mesh copper grid that had been previously glow-discharged. For negative staining, samples were stained with an aqueous 1% uranyl acetate solution prior to deposition. Particle sizes were analyzed from the images using ImageJ software.[61]

Powder X-ray Diffraction. AgNP samples were lyophilized overnight, and the resulting powder was spread out with a thin layer of oil on a glass slide. X-ray diffraction spectra were acquired at UBC's Department of Chemistry on a Bruker D8 Advance X-ray diffractometer (Billerica, MA).

AgNP Serum Stability. AgNPs were dissolved in either water or mouse serum to a concentration of 0.5 mg/mL in a dynamic laser light scattering (DLS) cuvette. Samples were incubated at 37 °C, and the hydrodynamic diameter was measured by DLS at each time point.

Animal Care and Ethics. Animal experiments were performed in accordance with the Canadian Council on Animal Care (CCAC) guidelines. All protocols were approved by the University of British Columbia Animal Care Committee. All mice were obtained from Charles River Laboratories. For the imaging study, healthy female C57BL/6 mice (22.0 ± 2.5 g) at the age of 19 weeks old were used. For the infection model study, healthy female CD-1 mice (25 ± 5 g) at the age of 7−8 weeks were used. Special care was taken to prevent contact between infected and noninfected mice. All animals were housed in cohorts of 4, and standard animal husbandry protocols were employed.

SPECT/CT Acquisition. The procedure used for intratracheal instillation (IT) has been described in detail previously.[62] Prior to IT, healthy female C57BL/6 mice (19 weeks old) were anesthetized using isoflurane via inhalation (5% in oxygen) in an induction chamber. [[111]Ag]AgNPs were diluted to a concentration of 592 MBq/mL (4.0 mg/mL) in water on the day of the animal study, and 25 μL of this

solution was administrated directly to the trachea using a glass syringe equipped with a blunt-tipped 22G catheter (BD Insyte Autoguard shielded IV catheter, BD Biosciences, San Jose, CA). The administered dose was determined by measuring the radioactivity in the syringe before and after administration. Thereafter, the mice were transferred to the animal imaging bed and static SPECT images were acquired at 0.2, 0.4, 2, 5, 24, and 48 h using a preclinical VECTor/CT scanner[63] (MILabs, Utrecht, The Netherlands) equipped with a high-energy ultrahigh-resolution mouse pinhole collimator (HE-UHR-1.0 mm). CT scans were acquired with a tube setting of 55 kV and 615 μA. During the entire scanning procedure, the mice were kept under anesthesia with 1.5−2% isoflurane in oxygen, and the body temperature was maintained constant using an integrated heating pad in the scan bed. After each scan, the animals were recovered individually with heat support and nearby access to a HydroGel gel-based water source (ClearH2O, Portland, ME). Once recuperated from anesthesia, the animals were returned to their normal group housing until their next scan.

Images were reconstructed using pixel-based ordered-subset expectation maximization (POSEM)[64] algorithm using 16 subsets, six iterations, and an isotropic 0.4 mm voxel grid. The energy photopeak for ^{111}Ag was centered at 342 keV $\pm$ 12.5% (25%). All images were decay-corrected and, using the CT image, attenuation correction was applied. To convert the reconstructed SPECT images to activity concentration, a calibration factor was determined by scanning a point-source phantom with a known concentration of ^{111}Ag, following the procedure described by Wu et al.[65]

SPECT/CT Image Analysis. The obtained SPECT/CT images were analyzed using AMIDE,[66] a public domain software for medical imaging data, which was used to generate maximum intensity projections (MIPs) as well as for placing and analyzing volumes of interest (VOIs). VOIs were manually drawn inside each tissue/organ using the CT image to determine the time−activity pattern per target organ or tissue. The main interest regions were the right and left lungs. Additional analysis of the mouth and the trachea was conducted to quantify the residual activity in those areas.

Biodistribution Study. Following the terminal SPECT/CT scan at 48 h post administration, the mice were euthanized by CO_2 asphyxiation under isoflurane anesthesia. The cardiac puncture was promptly performed to recover blood, and the organs of interest detailed in Table S2 were harvested. Each organ was weighed, and its ^{111}Ag was activity measured on a calibrated γ counter (Packard Cobra II Autogamma counter, PerkinElmer, Waltham, MA) using an energy window from 280 to 400 keV. The amount of ^{111}Ag in each organ was decay-corrected and expressed as the percentage of the administered dose per gram (% AD/g) and per organ (% AD/organ).

Bacterial Growth Conditions. All bacteria were streaked onto Luria−Bertani broth (LB) agar plates (Thermo Fisher Scientific) from frozen stocks and grown overnight at 37 °C. The following day, an individual colony was used to make an overnight culture in LB broth by incubating at 37 °C with shaking at 250 rpm for 16−18 h. Bacterial growth was monitored by measuring the optical density with a spectrophotometer (Eppendorf) at 600 nm (OD600). Subcultures were achieved by diluting overnight bacterial cultures to OD600 = 0.1 and growing to an OD600 = 1. Bacterial subcultures were washed twice with sterile PBS and resuspended in appropriate media.

Minimal Inhibitory Concentration (MIC) and Minimal Bactericidal Concentration (MBC). MIC and MBC were performed similarly to what was described previously.[32] Briefly, the activity of the AgNPs was tested against the Gram-positive isolate *S. aureus* USA300 (CDC, 2003) and various Gram-negative isolates, including *A. baumannii* (ATCC BAA-747), *Klebsiella pneumoniae* 124, *P. aeruginosa* strain LESB58,[67] *P. aeruginosa* LESB65,[43] and *P. aeruginosa* PA01. All bacteria were grown as described above.

Testing was done in round-bottom 96 well plates with 50% Mueller−Hinton broth with either 50% PBS or water and an inoculum that yielded a final optical density at 600 nm (OD600) of 0.05. Nanoparticles were added in a range of 0.25−128 μg/mL into a total volume of 100 μL. Microplates were shaken at 37 °C for 24 h. Turbidity or cell pellets indicated bacterial growth. The first well

without visible growth was determined as the MIC. To determine the MBC, 10 μL of each well from the MIC plate was plated onto LB agar plates and incubated for an additional 24 h at 37 °C. All tests were performed at least in triplicates.

***In Vivo* Intranasal Infection Model.** The intranasal infection model was performed as previously described.[43] Briefly, *P. aeruginosa* LESB65 subcultures were washed twice with sterile PBS and further adjusted to 0.5 × 10^9 CFU/mL. Twenty microliters (20 μL) of bacteria were instilled into the left naris of female CD-1 mice under anesthesia (2.5% isoflurane). Animals were monitored and given heat support immediately following the infection. All animals were allowed to recover from anesthesia before returning to cages. Mice were treated with endotoxin-free water (vehicle control) or 0.5, 1.67, or 5 mg/kg AgNPs 24 h post infection.

At the experimental end point 24 h after infection, mice were euthanized by intraperitoneal injection of sodium pentobarbital (120 mg/kg), followed by cardiac puncture. Whole lungs were collected in sterile PBS and homogenized using Mini Beadbeater-96 cell disrupter (BioSpec Products) for 5 min. Serial dilutions of lung homogenates were used to enumerate bacterial burden, and the remaining liquid was stored at −200 °C until further use in protein quantification via ELISA according to the manufacturers' descriptions. Fold changes in bacterial burden were calculated as the geometric mean CFU per gram of lung tissue in the vehicle control group divided by the geometric mean CFU per gram of lung tissue in the treatment group. IL-6 was determined with a mouse assay (Cat14-7061-81 and 13-7062-81; Thermo Fisher, Burnaby, BC, Canada) and IL-1α as well (Cat# DY400, R&D Systems Inc., Minneapolis, MN). The chemokine KC was analyzed with a CXCL1/KC duo set assay (Cat# DY453-05, R&D Systems Inc., Minneapolis, MN), and the chemokine MCP-1 (Cat# 14-7091-81 and 13-7096, Thermo Fisher, Burnaby, BC, Canada), with a monoclonal antibody assay.

Statistical Analysis. Unless stated otherwise, all data are presented as the arithmetic mean $\pm$ 1 standard deviation. Prism 9 software (GraphPad, San Diego, CA) was used to perform all statistical tests. All experiments were performed at least in triplicate.

■ ASSOCIATED CONTENT

Ⓢ Supporting Information

The Supporting Information is available free of charge at https://pubs.acs.org/doi/10.1021/acsami.2c03609.

Figures showing changes in AgNP antimicrobial activity with storage, the comprehensive biodistribution of [^{111}Ag]AgNPs, PXRD spectrum of AgNPs, separation of silver from palladium, changes in AgNP diameter with storage, the hydrodynamic diameter of AgNPs in different conditions, and changes in AgNP hydrodynamic diameter in different conditions (PDF)

■ AUTHOR INFORMATION

Corresponding Authors

Katayoun Saatchi − *Faculty of Pharmaceutical Sciences, University of British Columbia, Vancouver, BC V6T1Z3, Canada;* ⓞ orcid.org/0000-0002-5372-6791; Email: kathy.saatchi@ubc.ca

Urs O. Häfeli − *Faculty of Pharmaceutical Sciences, University of British Columbia, Vancouver, BC V6T1Z3, Canada; Department of Pharmacy, Faculty of Health and Medical Sciences, University of Copenhagen, Copenhagen 2100, Denmark;* ⓞ orcid.org/0000-0003-0671-4509; Email: urs.hafeli@ubc.ca

Authors

Colin Blackadar − *Faculty of Pharmaceutical Sciences, University of British Columbia, Vancouver, BC V6T1Z3, Canada;* ⓞ orcid.org/0000-0002-3847-3693

Ka-Yee Grace Choi − *Centre for Microbial Diseases and Immunity Research, Department of Microbiology and Immunology, Faculty of Science, University of British Columbia, Vancouver, BC V6T1Z4, Canada;* ◉ orcid.org/0000-0002-6320-9915

Mary F. Embree − *University of Missouri Research Reactor Center (MURR), Columbia, Missouri 65211, United States*

Heather M. Hennkens − *University of Missouri Research Reactor Center (MURR), Columbia, Missouri 65211, United States; Department of Chemistry, University of Missouri, Columbia, Missouri 65211, United States;* ◉ orcid.org/0000-0002-3283-8751

Cristina Rodríguez-Rodríguez − *Faculty of Pharmaceutical Sciences, University of British Columbia, Vancouver, BC V6T1Z3, Canada; Department of Physics and Astronomy, University of British Columbia, Vancouver, BC V6T1Z1, Canada;* ◉ orcid.org/0000-0002-3313-4422

Robert E. W. Hancock − *Centre for Microbial Diseases and Immunity Research, Department of Microbiology and Immunology, Faculty of Science, University of British Columbia, Vancouver, BC V6T1Z4, Canada;* ◉ orcid.org/0000-0001-5989-8503

Complete contact information is available at:
https://pubs.acs.org/10.1021/acsami.2c03609

Author Contributions

K.S. and U.O.H. conceptualized the project. U.O.H. and R.E.W.H. provided financial support. C.B. synthesized and characterized the AgNPs. M.E. and H.H. prepared [111]Ag. C.B. and C.R.R performed SPECT/CT and biodistribution experiments. K.G.C. performed *in vitro* and *in vivo* characterizations of the AgNP antimicrobial activities. C.B. drafted the manuscript. All authors contributed to the manuscript revisions.

Notes

The authors declare no competing financial interest.

■ REFERENCES

(1) Siddiqi, K. S.; Husen, A.; Rao, R. A. K. A review on biosynthesis of silver nanoparticles and their biocidal properties. *J. Nanobiotechnol.* **2018**, *16*, No. 14.

(2) Roy, A.; Bulut, O.; Some, S.; Mandal, A. K.; Yilmaz, M. D. Green synthesis of silver nanoparticles: biomolecule-nanoparticle organizations targeting antimicrobial activity. *RSC Adv.* **2019**, *9*, 2673−2702.

(3) Rak, M. J.; Friščić, T.; Moores, A. One-step, solvent-free mechanosynthesis of silver nanoparticle-infused lignin composites for use as highly active multidrug resistant antibacterial filters. *RSC Adv.* **2016**, *6*, 58365−58370.

(4) Ray, S.; Mohan, R.; Singh, J. K.; Samantaray, M. K.; Shaikh, M. M.; Panda, D.; Ghosh, P. Anticancer and Antimicrobial Metallopharmaceutical Agents Based on Palladium, Gold, and Silver N-Heterocyclic Carbene Complexes. *J. Am. Chem. Soc.* **2007**, *129*, 15042−15053.

(5) Ashraf, R.; Bhatti, H. N.; Iqbal, M. A.; Jamil, Y. Synthesis of aryl linked binuclear silver N-heterocyclic carbene complexes, DNA interaction study and biological potentials. *Inorg. Chem. Commun.* **2020**, *119*, No. 108077.

(6) Shah, P. N.; Lin, L. Y.; Smolen, J. A.; Tagaev, J. A.; Gunsten, S. P.; Han, D. S.; Heo, G. S.; Li, Y.; Zhang, F.; Zhang, S.; Wright, B. D.; Panzner, M. J.; Youngs, W. J.; Brody, S. L.; Wooley, K. L.; Cannon, C. L. Synthesis, characterization, and in vivo efficacy of shell cross-linked nanoparticle formulations carrying silver antimicrobials as aerosolized therapeutics. *ACS Nano* **2013**, *7*, 4977−4987.

(7) Lim, Y. H.; Tiemann, K. M.; Heo, G. S.; Wagers, P. O.; Rezenom, Y. H.; Zhang, S.; Zhang, F.; Youngs, W. J.; Hunstad, D. A.; Wooley, K. L. Preparation and in vitro antimicrobial activity of silver-bearing degradable polymeric nanoparticles of polyphosphoester-block-poly(L-lactide). *ACS Nano* **2015**, *9*, 1995−2008.

(8) Cao, F.; Ju, E.; Zhang, Y.; Wang, Z.; Liu, C.; Li, W.; Huang, Y.; Dong, K.; Ren, J.; Qu, X. An Efficient and Benign Antimicrobial Depot Based on Silver-Infused MoS2. *ACS Nano* **2017**, *11*, 4651−4659.

(9) Lu, X.; Ye, J.; Zhang, D.; Xie, R.; Bogale, R. F.; Sun, Y.; Zhao, L.; Zhao, Q.; Ning, G. Silver carboxylate metal−organic frameworks with highly antibacterial activity and biocompatibility. *J. Inorg. Biochem.* **2014**, *138*, 114−121.

(10) Lansdown, A. B. Silver in health care: antimicrobial effects and safety in use. *Curr. Probl. Dermatol.* **2006**, *33*, 17−34.

(11) Drake, P. L.; Hazelwood, K. J. Exposure-Related Health Effects of Silver and Silver Compounds: A Review. *Ann. Occup. Hyg.* **2005**, *49*, 575−585.

(12) AshaRani, P. V.; Low Kah Mun, G.; Hande, M. P.; Valiyaveettil, S. Cytotoxicity and Genotoxicity of Silver Nanoparticles in Human Cells. *ACS Nano* **2009**, *3*, 279−290.

(13) Braydich-Stolle, L.; Hussain, S.; Schlager, J. J.; Hofmann, M.-C. In vitro cytotoxicity of nanoparticles in mammalian germline stem cells. *Toxicol. Sci.* **2005**, *88*, 412−419.

(14) Hussain, S. M.; Hess, K. L.; Gearhart, J. M.; Geiss, K. T.; Schlager, J. J. In vitro toxicity of nanoparticles in BRL 3A rat liver cells. *Toxicol. in Vitro* **2005**, *19*, 975−983.

(15) Li, W. T.; Chang, H. W.; Chen, M. H.; Chiou, H. Y.; Liou, B. Y.; Pang, V. F.; Yang, W. C.; Jeng, C. R. Investigation of silver (Ag) deposition in tissues from stranded cetaceans by autometallography (AMG). *Environ. Pollut.* **2018**, *235*, 534−545.

(16) Lee, K. J.; Nallathamby, P. D.; Browning, L. M.; Osgood, C. J.; Xu, X.-H. N. In vivo imaging of transport and biocompatibility of single silver nanoparticles in early development of zebrafish embryos. *ACS Nano* **2007**, *1*, 133−143.

(17) Yan, N.; Tang, B. Z.; Wang, W.-X. In Vivo Bioimaging of Silver Nanoparticle Dissolution in the Gut Environment of Zooplankton. *ACS Nano* **2018**, *12*, 12212−12223.

(18) Zhang, X.; Yao, M. N.; Chen, M. H.; Li, L. Q.; Dong, C. Y.; Hou, Y.; Zhao, H. Y.; Jia, B.; Wang, F. Hyaluronic Acid-Coated Silver Nanoparticles As a Nanoplatform for in Vivo Imaging Applications. *ACS Appl. Mater. Interfaces* **2016**, *8*, 25650−25653.

(19) Chrastina, A.; Schnitzer, J. E. Iodine-125 radiolabeling of silver nanoparticles for in vivo SPECT imaging. *Int. J. Nanomed.* **2010**, *5*, 653−659.

(20) Tan, X.; Wang, J.; Pang, X.; Liu, L.; Sun, Q.; You, Q.; Tan, F.; Li, N. Indocyanine Green-Loaded Silver Nanoparticle@Polyaniline Core/Shell Theranostic Nanocomposites for Photoacoustic/Near-Infrared Fluorescence Imaging-Guided and Single-Light-Triggered Photothermal and Photodynamic Therapy. *ACS Appl. Mater. Interfaces* **2016**, *8*, 34991−35003.

(21) Xiu, Z.-m.; Zhang, Q.-b.; Puppala, H. L.; Colvin, V. L.; Alvarez, P. J. J. Negligible Particle-Specific Antibacterial Activity of Silver Nanoparticles. *Nano Lett.* **2012**, *12*, 4271−4275.

(22) Yang, X.; Gondikas, A. P.; Marinakos, S. M.; Auffan, M.; Liu, J.; Hsu-Kim, H.; Meyer, J. N. Mechanism of Silver Nanoparticle Toxicity Is Dependent on Dissolved Silver and Surface Coating in Caenorhabditis elegans. *Environ. Sci. Technol.* **2012**, *46*, 1119−1127.

(23) Alonso, M. J.; Gaspar, M. M.; Blanco, M. D.; Cruz, M. E. M. In *Development of PLGA nanospheres containing a high loading of L-asparaginase*, Proceedings of International Symposium on Controlled Release of Bioactive Materials; IEEE, 1996; pp 831−832.

(24) Mastren, T.; Radchenko, V.; Engle, J. W.; Weidner, J. W.; Owens, A.; Wyant, L. E.; Copping, R.; Brugh, M.; Nortier, F. M.; Birnbaum, E. R.; John, K. D.; Fassbender, M. E. Chromatographic separation of the theranostic radionuclide 111Ag from a proton irradiated thorium matrix. *Anal. Chim. Acta* **2018**, *998*, 75−82.

(25) Khalid, M.; Mushtaq, A.; Iqbal, M. Z. Separation of 111Ag from neutron irradiated natural palladium using alumina as an adsorbent. *Appl. Radiat. Isot.* **2000**, *52*, 19−22.

(26) Lyle, S. J.; Maghzian, R. Separation of carrier-free silver from neutron-irradiated palladium. *Talanta* **1968**, *15*, 712−713.

(27) Aweda, T. A.; Zhang, S.; Mupanomunda, C.; Burkemper, J.; Heo, G. S.; Bandara, N.; Lin, M.; Cutler, C. S.; Cannon, C. L.; Youngs, W. J.; Wooley, K. L.; Lapi, S. E. Investigating the pharmacokinetics and biological distribution of silver-loaded poly-phosphoester-based nanoparticles using (111) Ag as a radiotracer. *J. Labelled Compd. Radiopharm.* **2015**, *58*, 234−241.

(28) Aweda, T. A.; Ikotun, O.; Mastren, T.; Cannon, C. L.; Wright, B.; Youngs, W. J.; Cutler, C.; Guthrie, J.; Lapi, S. E. The use of (111) Ag as a tool for studying biological distribution of silver-based antimicrobials. *MedChemComm* **2013**, *4*, 1015−1017.

(29) Chattopadhyay, S.; Vimalnath, K. V.; Saha, S.; Korde, A.; Sarma, H. D.; Pal, S.; Das, M. K. Preparation and evaluation of a new radiopharmaceutical for radiosynovectomy, 111Ag-labelled hydrox-yapatite (HA) particles. *Appl. Radiat. Isot.* **2008**, *66*, 334−339.

(30) Sicilio, F.; Peterson, M. D.; Rudolph, G. G. Separation of Radioactive Silver-111 from Pile-Irradiated Palladium. *Anal. Chem.* **1956**, *28*, 365−366.

(31) National Center for Biotechnology Information; PubChem Compound Summary for CID 24947, Cadmium Chloride, 2021. https://pubchem.ncbi.nlm.nih.gov/compound/Cadmium-chloride.

(32) Pletzer, D.; Asnis, J.; Slavin, Y. N.; Hancock, R. E. W.; Bach, H.; Saatchi, K.; Häfeli, U. O. Rapid microwave-based method for the preparation of antimicrobial lignin-capped silver nanoparticles active against multidrug-resistant bacteria. *Int. J. Pharm.* **2021**, *596*, No. 120299.

(33) Thomas, N. C. Recovering silver nitrate from silver chloride residues in about thirty minutes. *J. Chem. Educ.* **1990**, *67*, No. 794.

(34) Willbanks, O. L. Reclaiming silver from silver chloride residues. *J. Chem. Educ.* **1953**, *30*, No. 347.

(35) von Dollen, J.; Oliva, S.; Max, S.; Esbenshade, J. Recovery of Silver Nitrate from Silver Chloride Waste. *J. Chem. Educ.* **2018**, *95*, 682−685.

(36) Das, R.; Nath, S. S.; Chakdar, D.; Gope, G.; Bhattacharjee, R. Synthesis of silver nanoparticles and their optical properties. *J. Exp. Nanosci.* **2010**, *5*, 357−362.

(37) Parvekar, P.; Palaskar, J.; Metgud, S.; Maria, R.; Dutta, S. The minimum inhibitory concentration (MIC) and minimum bactericidal concentration (MBC) of silver nanoparticles against *Staphylococcus aureus*. *Biomater. Invest. Dent.* **2020**, *7*, 105−109.

(38) Pareek, V.; Devineau, S.; Sivasankaran, S. K.; Bhargava, A.; Panwar, J.; Srikumar, S.; Fanning, S. Silver Nanoparticles Induce a Triclosan-Like Antibacterial Action Mechanism in Multi-Drug Resistant *Klebsiella pneumoniae*. *Front. Microbiol.* **2021**, *12*, No. 638640.

(39) Pritchard, J. N.; Holmes, A.; Evans, J. C.; Evans, N.; Evans, R. J.; Morgan, A. The distribution of dust in the rat lung following administration by inhalation and by single intratracheal instillation. *Environ. Res.* **1985**, *36*, 268−297.

(40) Anderson, D. S.; Silva, R. M.; Lee, D.; Edwards, P. C.; Sharmah, A.; Guo, T.; Pinkerton, K. E.; Van Winkle, L. S. Persistence of silver nanoparticles in the rat lung: Influence of dose, size, and chemical composition. *Nanotoxicology* **2015**, *9*, 591−602.

(41) Anderson, D. S.; Patchin, E. S.; Silva, R. M.; Uyeminami, D. L.; Sharmah, A.; Guo, T.; Das, G. K.; Brown, J. M.; Shannahan, J.; Gordon, T.; Chen, L. C.; Pinkerton, K. E.; Van Winkle, L. S. Influence of particle size on persistence and clearance of aerosolized silver nanoparticles in the rat lung. *Toxicol. Sci.* **2015**, *144*, 366−381.

(42) Kreyling, W. G.; Holzwarth, U.; Haberl, N.; Kozempel, J.; Wenk, A.; Hirn, S.; Schleh, C.; Schäffler, M.; Lipka, J.; Semmler-Behnke, M.; Gibson, N. Quantitative biokinetics of titanium dioxide nanoparticles after intratracheal instillation in rats: Part 3. *Nano-toxicology* **2017**, *11*, 454−464.

(43) Alford, M. A.; Choi, K. G.; Trimble, M. J.; Masoudi, H.; Kalsi, P.; Pletzer, D.; Hancock, R. E. W. Murine Model of Sinusitis Infection for Screening Antimicrobial and Immunomodulatory Therapies. *Front. Cell. Infect. Microbiol.* **2021**, *11*, No. 621081.

(44) Zhen, J.-B.; Kang, P.-W.; Zhao, M.-H.; Yang, K.-W. Silver Nanoparticle Conjugated Star PCL-b-AMPs Copolymer as Nano-composite Exhibits Efficient Antibacterial Properties. *Bioconjugate Chem.* **2020**, *31*, 51−63.

(45) Haidari, H.; Bright, R.; Garg, S.; Vasilev, K.; Cowin, A. J.; Kopecki, Z. Eradication of Mature Bacterial Biofilms with Concurrent Improvement in Chronic Wound Healing Using Silver Nanoparticle Hydrogel Treatment. *Biomedicines* **2021**, *9*, No. 1182.

(46) Escárcega-González, C. E.; Garza-Cervantes, J. A.; Vázquez-Rodríguez, A.; Montelongo-Peralta, L. Z.; Treviño-González, M. T.; Díaz Barriga Castro, E.; Saucedo-Salazar, E. M.; Chávez Morales, R. M.; Regalado Soto, D. I.; Treviño González, F. M.; Carrazco Rosales, J. L.; Cruz, R. V.; Morones-Ramírez, J. R. In vivo antimicrobial activity of silver nanoparticles produced via a green chemistry synthesis using Acacia rigidula as a reducing and capping agent. *Int. J. Nanomed.* **2018**, *13*, 2349−2363.

(47) Hindi, K. M.; Ditto, A. J.; Panzner, M. J.; Medvetz, D. A.; Han, D. S.; Hovis, C. E.; Hilliard, J. K.; Taylor, J. B.; Yun, Y. H.; Cannon, C. L.; Youngs, W. J. The antimicrobial efficacy of sustained release silver-carbene complex-loaded L-tyrosine polyphosphate nanopar-ticles: characterization, in vitro and in vivo studies. *Biomaterials* **2009**, *30*, 3771−3779.

(48) Gnanadhas, D. P.; Ben Thomas, M.; Thomas, R.; Raichur, A. M.; Chakravortty, D. Interaction of silver nanoparticles with serum proteins affects their antimicrobial activity in vivo. *Antimicrob. Agents Chemother.* **2013**, *57*, 4945−4955.

(49) Wu, L.; Rodríguez-Rodríguez, C.; Cun, D.; Yang, M.; Saatchi, K.; Häfeli, U. O. Quantitative comparison of three widely-used pulmonary administration methods in vivo with radiolabeled inhalable nanoparticles. *Eur. J. Pharm. Biopharm.* **2020**, *152*, 108−115.

(50) Hasegawa-Baba, Y.; Kubota, H.; Takata, A.; Miyagawa, M. Intratracheal instillation methods and the distribution of administered material in the lung of the rat. *J. Toxicol. Pathol.* **2014**, *27*, 197−204.

(51) Takenaka, S.; Karg, E.; Roth, C.; Schulz, H.; Ziesenis, A.; Heinzmann, U.; Schramel, P.; Heyder, J. Pulmonary and systemic distribution of inhaled ultrafine silver particles in rats. *Environ. Health Perspect.* **2001**, *109*, 547−551.

(52) Wiemann, M.; Vennemann, A.; Blaske, F.; Sperling, M.; Karst, U. Silver Nanoparticles in the Lung: Toxic Effects and Focal Accumulation of Silver in Remote Organs. *Nanomaterials* **2017**, *7*, No. 441.

(53) Morris, D.; Ansar, M.; Speshock, J.; Ivanciuc, T.; Qu, Y.; Casola, A.; Garofalo, R. Antiviral and Immunomodulatory Activity of Silver Nanoparticles in Experimental RSV Infection. *Viruses* **2019**, *11*, No. 732.

(54) Haberl, N.; Hirn, S.; Wenk, A.; Diendorf, J.; Epple, M.; Johnston, B. D.; Krombach, F.; Kreyling, W. G.; Schleh, C. Cytotoxic and proinflammatory effects of PVP-coated silver nanoparticles after intratracheal instillation in rats. *Beilstein J. Nanotechnol.* **2013**, *4*, 933−940.

(55) Silva, R. M.; Anderson, D. S.; Franzi, L. M.; Peake, J. L.; Edwards, P. C.; Van Winkle, L. S.; Pinkerton, K. E. Pulmonary effects of silver nanoparticle size, coating, and dose over time upon intratracheal instillation. *Toxicol. Sci.* **2015**, *144*, 151−162.

(56) Botelho, D.; Leo, B. F.; Massa, C.; Sarkar, S.; Tetley, T.; Chung, K. F.; Chen, S.; Ryan, M. P.; Porter, A.; Atochina-Vasserman, E. N.; Zhang, J.; Schwander, S.; Gow, A. J. Exposure to Silver Nanospheres Leads to Altered Respiratory Mechanics and Delayed Immune Response in an in Vivo Murine Model. *Front. Pharmacol.* **2018**, *9*, No. 213.

(57) Lee, J.; Cacalano, G.; Camerato, T.; Toy, K.; Moore, M. W.; Wood, W. I. Chemokine binding and activities mediated by the mouse IL-8 receptor. *J. Immunol.* **1995**, *155*, 2158−2164.

(58) Stebounova, L. V.; Adamcakova-Dodd, A.; Kim, J. S.; Park, H.; O'Shaughnessy, P. T.; Grassian, V. H.; Thorne, P. S. Nanosilver induces minimal lung toxicity or inflammation in a subacute murine inhalation model. *Part. Fibre Toxicol.* **2011**, *8*, No. 5.

(59) Botelho, D. J.; Leo, B. F.; Massa, C. B.; Sarkar, S.; Tetley, T. D.; Chung, K. F.; Chen, S.; Ryan, M. P.; Porter, A. E.; Zhang, J.; Schwander, S. K.; Gow, A. J. Low-dose AgNPs reduce lung mechanical function and innate immune defense in the absence of cellular toxicity. *Nanotoxicology* **2016**, *10*, 118−127.

(60) Yoksan, R.; Chirachanchai, S. Silver nanoparticles dispersing in chitosan solution: Preparation by γ-ray irradiation and their antimicrobial activities. *Mater. Chem. Phys.* **2009**, *115*, 296−302.

(61) Collins, T. J. ImageJ for microscopy. *BioTechniques* **2007**, *43*, S25−S30.

(62) Wu, L.; Rodriguez-Rodriguez, C.; Cun, D.; Yang, M.; Saatchi, K.; Häfeli, U. O. Quantitative Comparison of Three Widely-Used Pulmonary Administration Methods In Vivo with Radiolabeled Inhalable Nanoparticles. *Eur. J. Pharm. Biopharm.* **2020**, *152*, 108−115.

(63) Goorden, M. C.; van der Have, F.; Kreuger, R.; Ramakers, R. M.; Vastenhouw, B.; Burbach, J. P. H.; Booij, J.; Molthoff, C. F. M.; Beekman, F. J. VECTor: A Preclinical Imaging System for Simultaneous Submillimeter SPECT and PET. *J. Nucl. Med.* **2013**, *54*, 306−312.

(64) Branderhorst, W.; Vastenhouw, B.; Beekman, F. J. Pixel-based subsets for rapid multi-pinhole SPECT reconstruction. *Phys. Med. Biol.* **2010**, *55*, 2023−2034.

(65) Wu, C.; van der Have, F.; Vastenhouw, B.; Dierckx, R. A.; Paans, A. M.; Beekman, F. J. Absolute quantitative total-body small-animal SPECT with focusing pinholes. *Eur. J. Nucl. Med. Mol. Imaging* **2010**, *37*, 2127−2135.

(66) Loening, A. M.; Gambhir, S. S. AMIDE: A Free Software Tool for Multimodality Medical Image Analysis. *Mol. Imaging* **2003**, *2*, No. 153535002003031.

(67) Cheng, K.; Smyth, R. L.; Govan, J. R.; Doherty, C.; Winstanley, C.; Denning, N.; Heaf, D. P.; van Saene, H.; Hart, C. A. Spread of beta-lactam-resistant *Pseudomonas aeruginosa* in a cystic fibrosis clinic. *Lancet* **1996**, *348*, 639−642.